International Journal of Coal Science & Technology (2022) 9:62
https://doi.org/10.1007/s40789-022-00535-8

RESEARCH

# Semi-enclosed experimental system for coal spontaneous combustion for determining regional distribution of high-temperature zone of coal fire

**Jingyu Zhao[1,2,3] · Hanqi Ming[1] · Tao Guo[4] · Yuxuan Zhang[5] · Jun Deng[1,2] · Jiajia Song[1] · Qiang Zeng[3] · Chi-Min Shu[6]**

Received: 27 October 2021 / Accepted: 2 August 2022


**Abstract**

Temperature variation and gas generation at different depths and positions in the coal combustion process were studied to determine the propagation and evolution of high temperature regions in the process of coal spontaneous combustion. This study selected coal samples from Mengcun, Shaanxi Province, People's Republic of China, and developed a semi-enclosed experimental system (furnace) for simulating coal combustion. The thermal mass loss of coal samples under various heating rates (5, 10, and 15 °C/min) was analyzed through thermogravimetric analysis, and the dynamic characteristics of the coal samples were analyzed; the reliability of the semi-enclosed experimental system was verified through the equal proportional method of fuzzy response. The results reveal that the high-temperature zone is distributed nonlinearly from the middle to the front end of the furnace, and the temperatures of points in this zone decreased gradually as the layer depth increased. The apparent activation energy of the coal samples during combustion first increased and then decreased as the conversion degree increased. Furthermore, the proportion of mass loss and the mass loss rate in the coal samples observed in the thermogravimetric experiment is consistent with that observed in the first and second stages of the experiment conducted using the semi-enclosed system. The research findings can provide a theoretical basis for the prevention and control of high-temperature zones in coal combustion.

**Keywords** Coalfield fire area · Fuzzy migration path · Semi-enclosed experimental system · Thermogravimetric analysis · Dynamic characteristics

✉ Jiajia Song
songjiajia07@sina.com

[1] School of Safety Science and Engineering, Xi'an University of Science & Technology, Xi'an 710054, China

[2] Shaanxi Key Laboratory of Prevention and Control of Coal Fire, Xi'an University of Science & Technology, Xi'an 710054, China

[3] Post-Doctoral Research Centre for Ecology, Institute for Arid Ecology and Environment, Xinjiang University, Urumqi 830046, China

[4] Xi'an High-Tech Zone Emergency Management Bureau, Xi'an 710065, China

[5] Shaanxi Coal Chemical Industry Technology Research Institute Co. Ltd., Xi'an 710065, China

[6] Department of Safety, Health, and Environmental Engineering, National Yunlin University of Science and Technology, Douliou 64002, Yunlin, Taiwan, China

## 1 Introduction

Coalfield fires severely affect the environment and cause substantial resource wastage (Onifade et al. 2020). The fires in coalfield areas negatively affect air quality, surface vegetation, and geological conditions to varying degrees (Fan and Liu 2021; Hao et al. 2016; Saini et al. 2016; Xu et al. 2018a, b; Xu et al. 2018a, b). A large amount of dust, carbon monoxide (CO), sulphur dioxide, and other toxic and harmful gases are discharged into the atmosphere, causing regional air pollution and endangering public health (Alipour et al. 2021; Gehin et al. 2016; Ma et al. 2019; Wang et al. 2020a, b; Zhao et al. 2020). Additionally, the heat generated by the oxidation combustion of coal diffuses to the surface, resulting in surface water loss, reduced fertility, vegetation destruction, and soil erosion (Zhao et al. 2019a, b; Xu et al. 2020). Some metallic and non-metallic minerals burn at high temperatures to form acid–base compounds, a process that affects the formation of underground voids in the coal

Published online: 25 August 2022

layer, causing geological disasters, such as surface subsidence, depressions, and landslides (Hao et al. 2020; Song et al. 2019; Stracher and Taylor 2004; Sun et al. 2020; Xiao et al. 2016; Xu et al. 2020). Because of the development of surface fissures, severe air leakage, and oxygen supply, shallow coal bodies oxidise and heat up, causing spontaneous combustion of coal (Song et al. 2021; Zhao et al. 2019a, b). With a continuous supply of oxygen, the spontaneous combustion range of such a coal body gradually expands; moreover, the high-temperature area progressively spreads, extending from the surface to an underground depth of up to > 200 m, which engenders a coalfield fire area. Coalfield fires can occur worldwide and pose a severe threat to public health and natural ecological environments (Elick 2013; Ide and Orrjr, 2011; Ma et al. 2020; Nyakundi 2014; Pandey et al. 2014; Roy et al. 2016; Wang et al. 2020a, b; Zhang et al. 2020).

Because China attaches great value to coalfield fire areas, the government has formulated policies and measures according to the actual conditions of the coalfields and has achieved positive results in the detection and prevention of coalfield fires. Numerous models have been established for simulating the development of temperature fields in coalfield fire areas. Xia et al. (2014) developed a coupled hydro-thermo-mechanical model for coal seam spontaneous combustion and simulated the relationship between coal body deformation and permeability and coal temperature during coal seam spontaneous combustion. Wessling et al. (2008) combined rock flow results with on-site temperature observation data and used finite element analysis software to simulate the mechanical and energy transfer processes involved in coal fires. Huang et al. (2001) established a two-dimensional (2D) mathematical model of underground coal fires and explored the distribution of the temperature field and gas.

It can be seen from chemistry that spontaneous combustion is a phenomenon in which substances oxidise in the air and burn automatically, while combustion is a chemical phenomenon in which substances oxidise violently and emit light and heat. Therefore, coal spontaneous combustion is the result of physical and chemical action caused by long-term contact between coal and oxygen in the air. Taraba and Michalec (2011) adopted software to simulate the oxidation process of coal remaining in a longwall goaf. They established an oxidation kinetic model of coal spontaneous combustion and investigated the relationship between propulsion in the working face and the location and temperature of high-temperature points in the goaf. Song et al. (2014) established a 2D unsteady model to simulate the influence of air leakage channels on the range and temperature of coal combustion areas. They observed that when the oxygen supply conditions in the coal combustion area were altered, the average airflow velocity in the high-temperature area tripled. Onifade et al. (2020) used thermogravimetric analysis (TGA) and Wits-Ehac test to predict the spontaneous combustion possibility of samples collected between coal seams. When exposed to oxygen in the air, coal and coal shale spontaneous combustion occurs between coal seams, and their inherent characteristics and spontaneous combustion tendency are exceedingly different among different coal seams. Wolf and Bruining (2007) divided the combustion zone into several categories according to the degree of damage and conducted a comparative analysis of the influence of roof permeability on the temperature field distribution of the fire zone; they established a 2D model of coal fire energy, concentration, and flow to describe the thermal power of the zone. Qin et al. (2016) proposed theoretical and geometric models of the high-temperature zone of coal fire by simulating the oxygen concentration and temperature distribution in a goaf. Rosema et al. (2001) established a mathematical model of coal spontaneous combustion to investigate the open-air spontaneous combustion process of coal remaining in coal mines and mine goafs; they also analysed the influence of environmental factors, such as sun exposure and atmospheric changes and of the inherent conditions of the coal body size on the spontaneous combustion process. Yuan and Smith (2007) established a computational fluid dynamics (CFD) model for the first time to simulate coal spontaneous combustion in two goafs with fixed longwall face extraction ventilation system. To simulate the spontaneous combustion of longwall goaf, the non-exhaust ventilation system with fixed longwall working face is also simulated by CFD. Song et al. (2020) tested the carbon emission factor of smouldering coal by a homemade experimental platform (to a scale of 1:20) for underground coal combustion. The test results demonstrated that the total carbon emissions increased with the coal carbon content; volatile content was determined to be a major factor affecting combustion behaviour and gas emissions. Tan et al. (2019) introduced the characteristics of the No. 1 well in the Fukang mining area. They used a comprehensive detection range method to identify five large fire areas; on the basis of the characteristics of these large-scale and complex coal fire areas, they formulated, designed, and applied a district fire extinguishing plan. Kuenzer et al. (2012) evaluated coal fire dynamics by using the high-resolution multispectral and panchromatic Quickbird data. They also conducted semi-structured interviews with members of the Wuda local mining bureau. They analysed the entire data collected and indicated that the Wuda coal fires tended to move eastward.

Because of the complexity of coal combustion conditions and the difficulty of determining the high-temperature zone of a fire, it is particularly difficult to detect the fire source in a coalfield fire area. Existing research results do not provide a sufficient understanding of the principle governing the development of medium- and high-temperature zones in coalfield fire areas. To solve this research gap, this paper started with finding a method that can truly simulate the coalfield fire area and independently developed a self-developed semi-enclosed experimental system to solve the problem of inaccurate laboratory data and large differences from field data. On this basis, this was combined with thermogravimetric (TG) analysis and dynamic characteristic analysis to investigate the development and distribution of high-temperature zones in coalfield fire areas. The results demonstrated the development and spread of the high-temperature zone in the coalfield fire area. The findings of this study can provide a theoretical basis for research on high-temperature point control technology and lay a theoretical foundation for underground coal fire source identification and inversion.

## 2 Experimental and calculation methods

### 2.1 Coal sample

The coal sample of Mengcun, Shaanxi Province, China is avnon-caking coal in bituminous coal, which belongs to low rank coal. It has the characteristics of low calorific value, low ignition point, large moisture, long combustion time and is not easy to extinguish. It is one of the most typical coals prone to spontaneous combustion. Low metamorphic bituminous coal accounts for 42.2% of China's coal resources, mainly distributed in Northwest China. Non-caking coal can be used as coal for power generation and gasification, as well as power and civil fuel. It is widely used, with large market demand and large mining volume. Therefore, it was selected in this paper to study the regional distribution of high temperature in coalfield fire area. The surface of Mengcun is covered with a large loess layer, and the cretaceous strata in the valley are relatively flat. The coal samples were extracted from the working face, sealed in cloth bags, and transported to the laboratory. Before the experiment, the samples were crushed to a particle size of 7–10 mm to examine the evolution of a coal fire, and a small quantity was crushed to a particle size of 0.125 mm for TG analysis. Fresh coal samples were crushed and ground in the air according to the method for preparation of coal sample (GB474–2008) of the People's Republic of China, and samples with a diameter of 80–120 mesh were selected for proximate analysis and elemental analysis; the results are summarised in Table 1.

### 2.2 Semi-enclosed experimental system

This study developed a semi-enclosed experimental system for simulating coal fires to explore the distribution of oxygen supply and high-temperature zones in the fires. The experimental system comprised the following elements: temperature control and monitoring component, hydraulic device, semi-enclosed furnace with five layers, gas collection and analysis module, and pollutant disposal module (Fig. 1). The external dimensions of the furnace were 600 mm × 600 mm × 730 mm, and the internal dimensions were 300 mm × 300 mm × 600 mm (Fig. 2). The furnace wall was composed of carbon steel and a high-temperature-resistant pure fibre blanket. Several through holes of diameter 16 mm were created on the wall that served as temperature and gas acquisition points. The temperature control and monitoring component controlled the heating temperature and time according to changes in the heat source temperature of the furnace. A stainless-steel gas tube extracted gases from the fire and injected them into the chromatograph for analysis of the oxygen concentration and gaseous products released in various directions during the fire. Heating rods, used to ignite the surface of the coal seam in the experiment, were inserted into the through holes in the second layer and were removed when the surface coal started burning.

The height of the coal body in the system was 470 mm, and the ambient temperature was 5 °C. The heating rods were arranged evenly on the surface of the coal, and the heating temperature was preset to 600 °C. The surface of the coal body started yielding yellow smoke and moisture after 13 min of heating. After 25 min, the surface of the coal first exhibited open fire, and the temperature of the coal had increased to 309.5 °C. The smoke exhibited distinct diffusion. The temperature of thermocouple No. 13 at the bottom of the furnace body was 300 °C after 26 h of heating. After 600 h, the temperature of all measuring points inside the furnace body remained constant.

### 2.3 Measuring point arrangement

Temperature and gas measuring units were arranged in the furnace to monitor changes in temperature and oxygen over time and across the coal fire area. Three measuring points were set in each layer of the furnace, and the distances between these points and the inner wall of the furnace were 50, 150, and

**Table 1** Proximate analysis and elemental analysis of coal samples

| Sample | Proximate analysis (%) | | | Ultimate analysis (%) | | | | |
|---|---|---|---|---|---|---|---|---|
| Mengcun | $M_{ad}$ | $A_{ad}$ | $V_{ad}$ | C | H | O | N | S |
| | 4.4 | 14.1 | 33.5 | 78.8 | 4.8 | 14.2 | 1.4 | 0.8 |

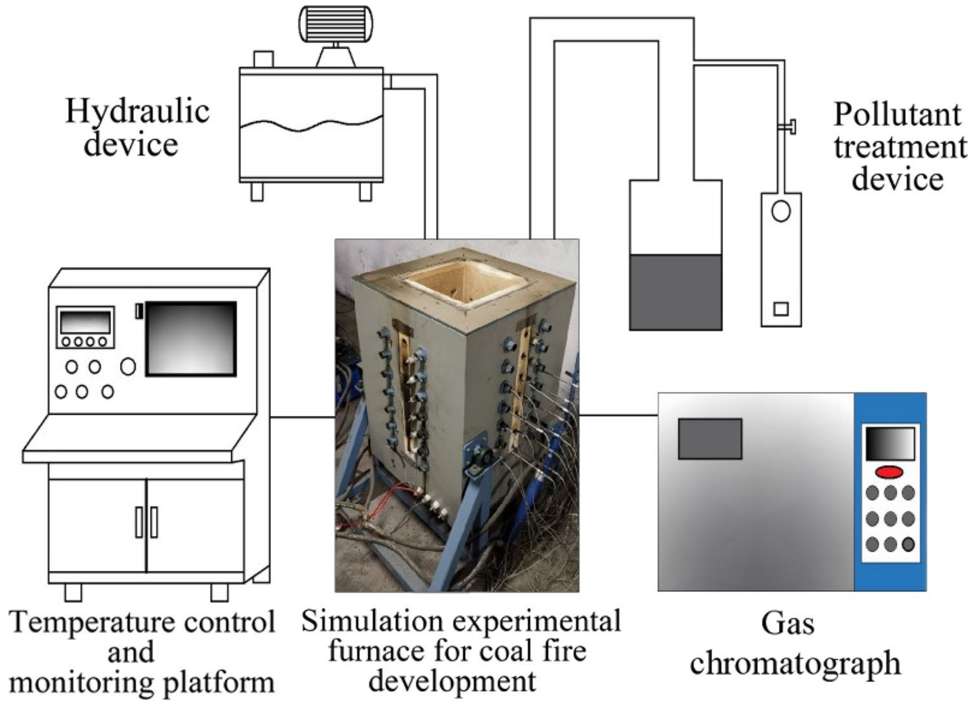


**Fig. 1** Semi-enclosed experimental system for simulating coal fires

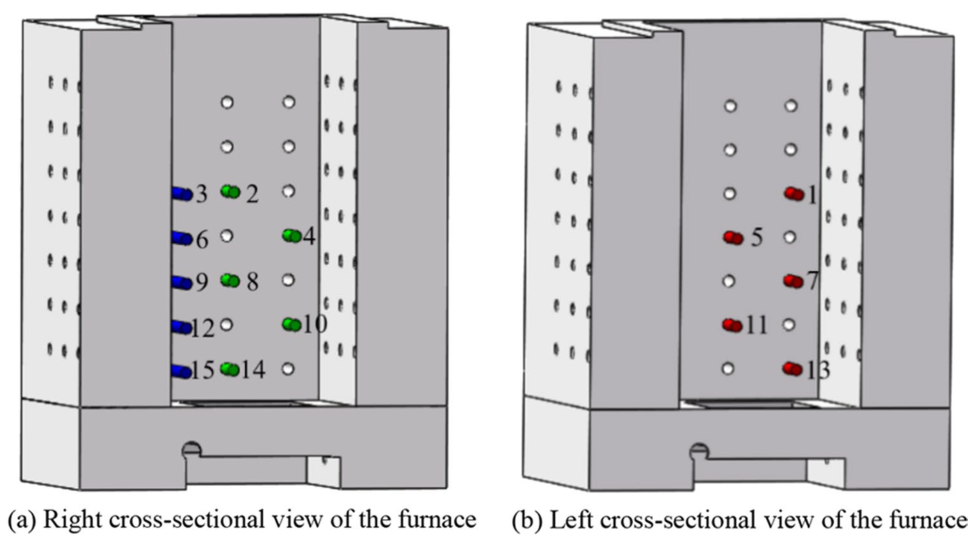


**Fig. 2** Measuring point layout for points Nos. 1 to 15

250 mm. Thus, a total of 15 measuring points were used in the five layers of the furnace. In addition, 16-mm-diameter thermocouples for temperature measurement and a 3-mm-diameter metal tube for gas extraction were placed in the through holes to monitor temperature and gas changes at various locations (Fig. 2a). Thermocouples 1, 4, 7, 10, and 13 (Fig. 2b, red) were at distances of 250, 50, 250, 50, and 250 mm, respectively, from the inner wall of the furnace; thermocouples 2, 5, 8, 11, and 14 (Fig. 2b, green) were at distances of 50, 250, 50, 250, and 50 mm, respectively, from the inner wall of the furnace; and thermocouples, 6, 9, 12, and 15 (Fig. 2b, blue) were all at a distance of 150 mm from the inner wall of the furnace. During the experiment, the unused holes were plugged with ceramic plug rods to prevent the leakage of air and the outflow of inflammable substances, such as tar.

### 2.4 TG experiment

TG analysis was conducted using the Labsys Evo Synchronous Thermal Analyser (Setaram, Inc., Lyon, France). The particle size of the samples used in the experiment was 120 mesh (0.125 mm), and the experimental dose was 5 mg. The temperature rise range for the experiment was 30–800 °C, and the gas flow rate was 50 mL/min. In the experiment, an

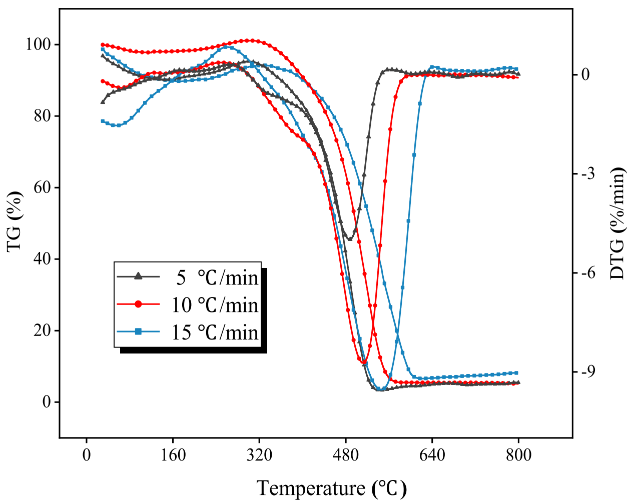


**Fig. 3** TG and DTG curves obtained for Mengcun coal samples under various heating rates

**Table 2** Characteristic temperatures of Mengcun coal samples under various heating rates by TG test

| Heating rate | 5 (°C/min) | 10 (°C/min) | 15 (°C/min) |
|---|---|---|---|
| $T_1$ (°C) | 65–80 | 65–80 | 55–70 |
| $T_2$ (°C) | 140–155 | 115–130 | 160–175 |
| $T_3$ (°C) | 165–180 | 165–180 | 200–215 |
| $T_4$ (°C) | 260–275 | 240–255 | 250–255 |
| $T_5$ (°C) | 295–310 | 295–310 | 320–335 |

oxygen–nitrogen mixed-gas cylinder with an external oxygen concentration of 21 rol% (approximating the air environment) was used, and the applied heating rates were 5, 10, and 15 °C/min.

## 3 Results and discussion

### 3.1 TG analysis

The TG and derivative TG (DTG) curves obtained for the Mengcun coal samples under various heating rates are presented in Fig. 3. According to a previously presented method for identifying characteristic temperature points (Zhao et al. 2019a, b), this study determined the characteristic temperature range for the samples under various heating rates, as listed in Table 2. As the heating rate increased, the critical temperature $T_1$ decreased, the dry cracking temperature $T_2$ and growth temperature $T_4$ first decreased and then increased, and the activity temperature $T_3$ and ignition temperature $T_5$ increased. A lower critical temperature is typically associated with an accelerated coal–oxygen recombination reaction. When the heating rate was 15 °C/min, the spontaneous combustion tendency of the coal samples was the highest. These results indicate that the heating rate clearly affected the adsorption–desorption and thermal decomposition reactions with high reaction intensity before the dry cracking temperature was reached. Therefore, the heating rate had the greatest impact on the dry cracking temperature. As the heating rate increased, the temperature difference between the ambient temperature and the coal sample temperature as well as the ambient air pressure increased rapidly; this was conducive to the diffusion of oxygen to the coal surface, the progress of the coal–oxygen reaction, and the formation of carbon and oxygen compounds, thus increasing the mass change rate. Concurrently, the time required for the temperature of the coal samples to reach the ambient temperature was shortened, and the coal–oxygen reaction required a certain time; therefore, the TG and DTG curves demonstrated a lag, and the combustion of the coal samples shifted to the high-temperature zone. When the combustion reached the high-temperature stage, the early lag effect was accumulated; consequently, the influence of the heating rate became clearer as the temperature increased.

### 3.2 Apparent activation energy

This study used the Kissinger–Akahira–Sunose (KAS) method to calculate the apparent activation energy of the Mengcun coal samples under various heating rates (Wang et al. 2018).

The dynamic equation is expressed as follows:

$$\ln\left(\frac{\beta}{T^2}\right) = -\left(\frac{E_a}{RT}\right) + \ln\left(\frac{AR}{g(\alpha)E_a}\right), \quad (1)$$

where, $\beta$ is the heating rate during the experiment (°C/min); $g(\alpha)$ is the integral expression of $1/f(\alpha)$, where $\alpha$ is the conversion degree (%); $A$ is the pre-exponential factor (1/s); $E_a$ is the apparent activation energy (J/mol); $R$ is the universal gas constant (8.314 J/K mol); and $T$ is the absolute temperature (K).

The KAS method was executed by setting conversion rate $\alpha$ to the range 0.1–0.9, setting $\ln(\beta/T^2)$ as the Y-axis, and setting 1000/$T$ as the $X$-axis (Fig. 4). The slope was determined through linear fitting, and the apparent activation energy corresponding to each conversion degree was then estimated. Through the KAS method, the average apparent activation energy was calculated to be 83.8 kJ/mol. As illustrated in Fig. 5, the apparent activation energy first increased and then decreased as the conversion degree increased. At the initial stage of oxidation, functional groups in coal that could easily react with oxygen initially reacted with oxygen to release heat. The number of active functional groups

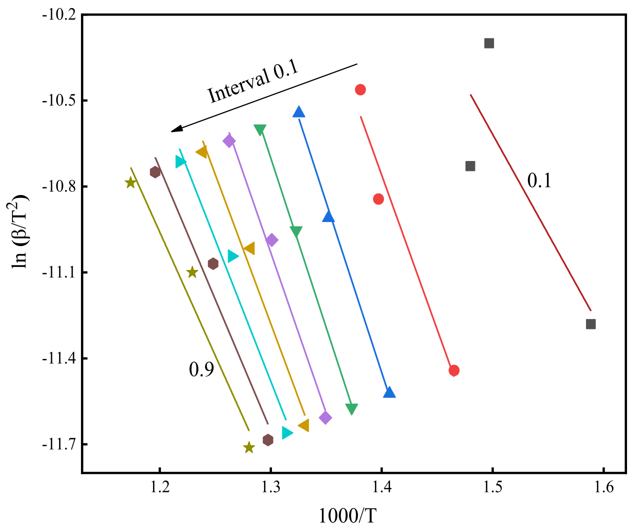


**Fig. 4** Linear regression executed using the KAS method under various conversion degrees

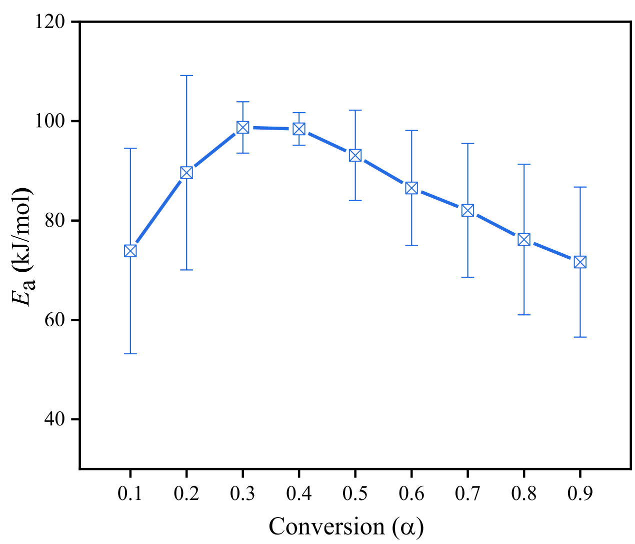


**Fig. 5** Change in apparent activation energy with conversion degree for Mengcun coal samples

participating in the reaction was small, the energy required was small, and the apparent activation energy was low. However, with the accumulation of heat and the increase in temperature, coal functional groups that could not readily react with oxygen at low temperatures were gradually activated and participated in the reaction, and the energy required was higher. Overall, on the basis of the variation of the apparent activation energy, this study considered that the thermal mass loss of coal in the semi-enclosed experimental system involved a reaction process from 0 to 1. The semi-enclosed experimental system was established to simulate the progression of coal from its spontaneous combustion to its extinction, which is consistent with the process of coal thermal analysis.

### 3.3 High-temperature zone distribution

Using CO as an indicator and applying growth rate analysis (Guo et al. 2019), this study determined the characteristic temperatures of the Mengcun coal samples, which are listed in Table 3.

The temperature variation observed at the 15 measuring points in the experimental furnace over time is illustrated in Fig. 6. As displayed in this figure, the variation trends were generally similar among the three measuring points in each layer. When the temperature at a measuring point exceeded the ignition temperature for the first time, the coal in the measuring point area reacted violently with oxygen, and the oxygen consumption rate was high; consequently, this measuring point was determined to be located in a high-temperature zone and to be the key point in this zone. In the early stage of this experiment, the temperature variation at each measuring point was small, and the temperature was essentially maintained at 4–6 °C, which was close to the ambient temperature. Among the 15 temperature measuring points on the five layers of the furnace, Nos. 2, 5, 7, 10, and 13 were the first to reach the characteristic temperature and required 5, 12, 15, 20, and 26 h, respectively, to reach the ignition temperature. Specifically, the peak temperatures at measuring points 2, 5, 7, 10, and 13 (i.e., the key points) were 624, 605, 528, 471, and 441 °C, respectively, and these points required 15, 24, 32, 40, and 68 h, respectively, to reach their peak temperatures.

According to the preceding analysis results, the high-temperature points developed from the middle of the furnace body and moved toward the front and, regarding the development of the high-temperature zone during the combustion process, the zone moved downward from points 2, 5, 7, 10, and 13, mainly in the middle and western directions. The fuzzy migration path of the high-temperature zone is shown in Fig. 7. The high-temperature zone first appeared 5 h after the start of the test at point No. 2, which was located 50 mm from the right side of the furnace. The surface coal sample was affected by the airflow. After ignition, the coal–oxygen

**Table 3** Characteristic temperatures of coal samples

| Item | Characteristic temperature (°C) |
|---|---|
| Critical temperature | 65–80 |
| Crack temperature | 115–130 |
| Active temperature | 165–180 |
| Speedup temperature | 235–250 |
| Ignition temperature | 295–310 |

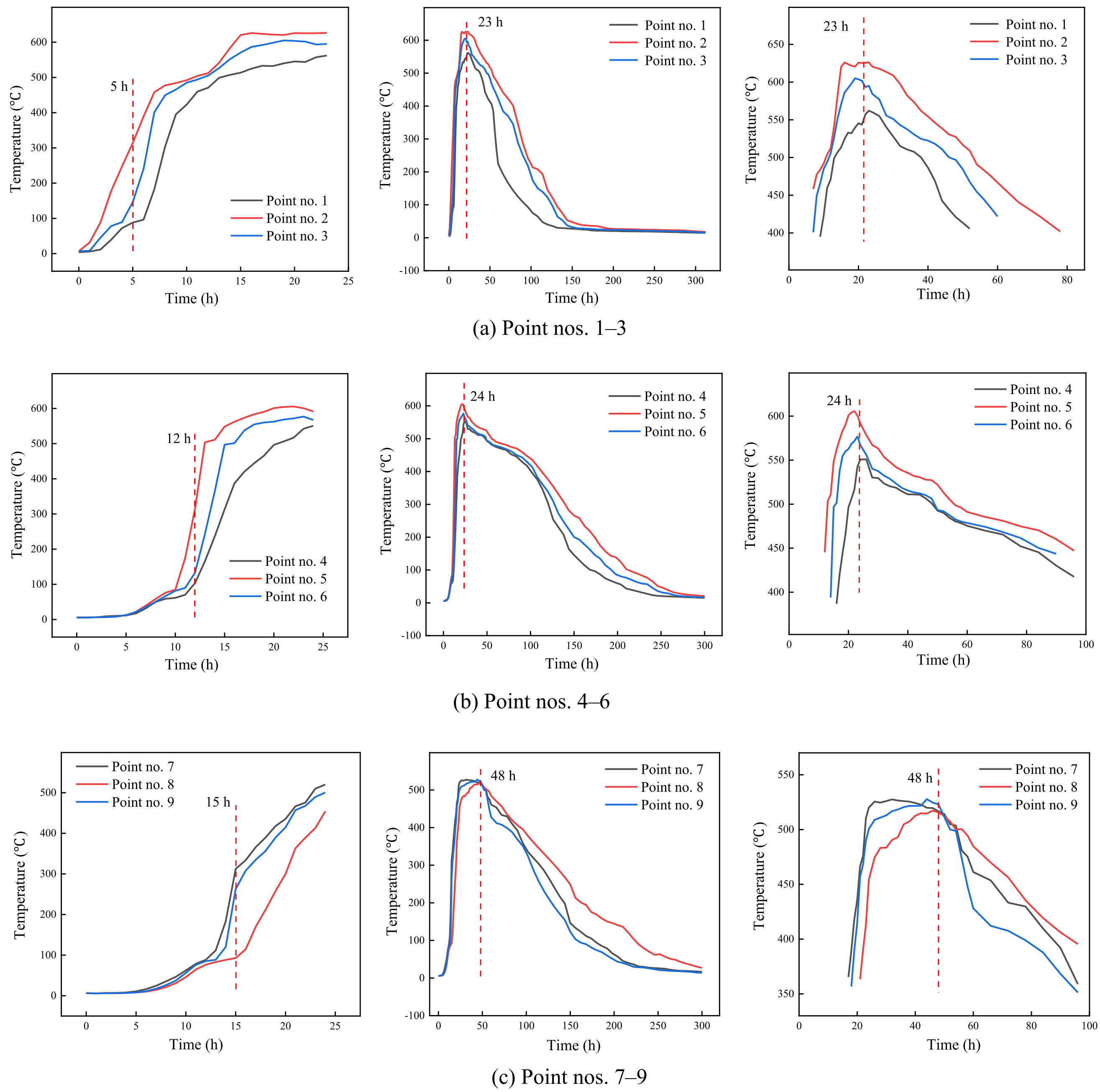


(a) Point nos. 1–3

(b) Point nos. 4–6

(c) Point nos. 7–9

**Fig. 6** Curve of temperature within 600 h of Mengcun coal sample combustion

reaction was accelerated, and the first high-temperature zone was formed. After 12 h, the high-temperature zone began to migrate to the left side of the furnace body and appeared at point No. 5, which was located 250 mm from the right side of the furnace. Because of the influence of the crack, after the combustion of the surface coal, the oxygen first propagated downward along the crack that was most readily diffused, resulting in the spontaneous combustion of the coal sample near the crack, an uncontrolled rise in the coal temperature to the ignition temperature, and uniform combustion of the second coal body under the influence of heat transfer. After 15 h, a high-temperature zone appeared at point No. 7 at the left front of the furnace body; the oxygen channel continued to move downward nonlinearly, and the high-temperature zone moved to the front end of the furnace body. The full combustion of the coal samples in the first and second layers of the furnace resulted in heat accumulation, which stimulated the prompt temperature rise at point No. 7, and the high-temperature point started to move vertically downward. After 20 h, the high-temperature

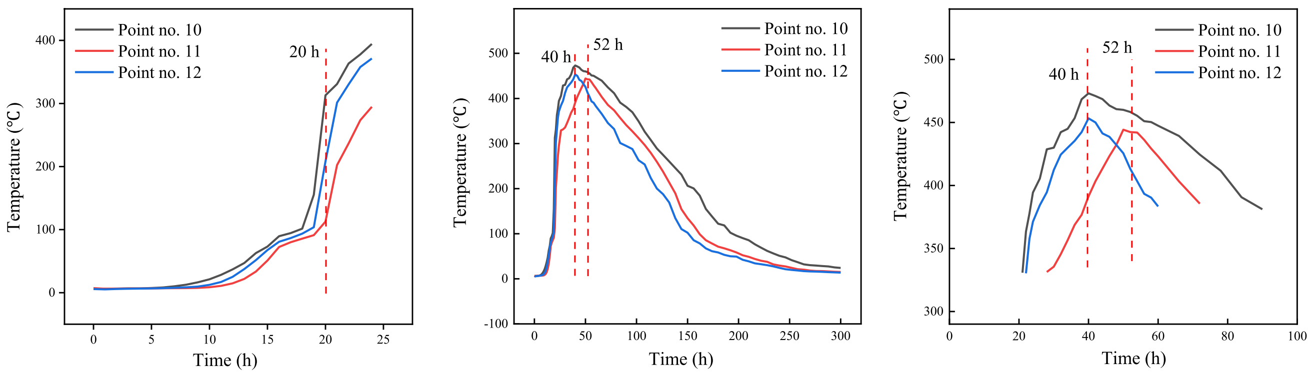


(d) Point nos. 10–12

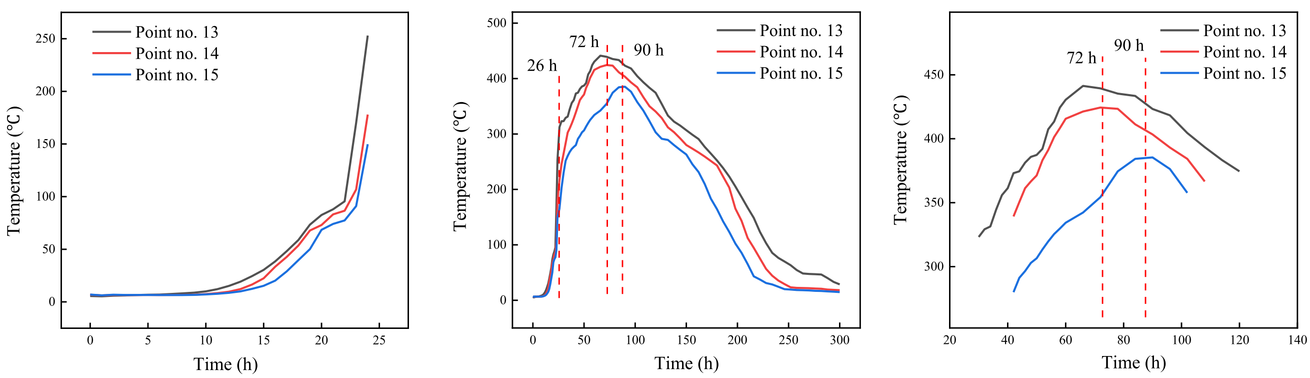


(e) Point nos. 13–15

**Fig. 6** (continued)

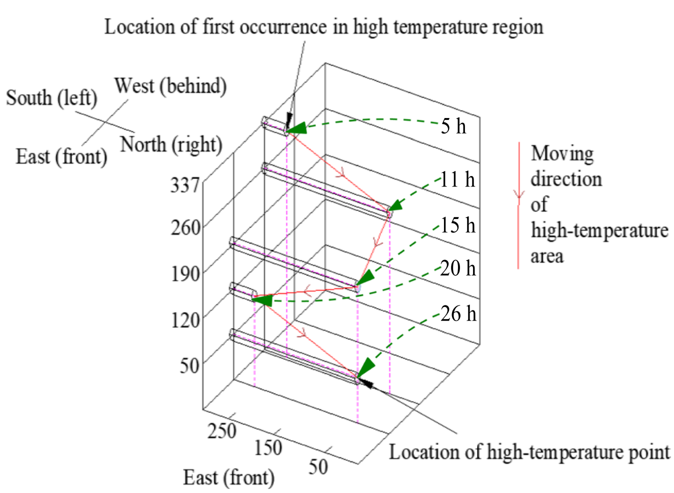


(a) Three-dimensional map

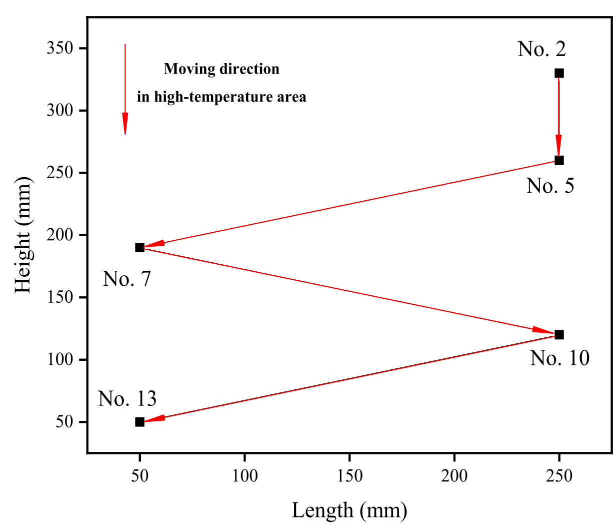


(b) Sectional schematic

**Fig. 7** High-temperature zone movement and distribution for Mengcun coal samples zone appeared near point No. 10, and the temperature at the bottom of the furnace started to rise slowly. After 26 h, the high-temperature zone emerged for the first time at point No. 13, which was located 50 mm from the bottom of the furnace and 250 mm from the left side of the furnace. The peak temperature decreased gradually as the depth increased, indicating that the actual temperature growth rate of the deep coal body differed from that of the shallow coal body. Regarding the temperature decrease in each layer, the decrease rate was the slowest at the key points in the high-temperature zone, and after the overall temperature dropped to 80 °C, the cooling rate at each measuring point was extremely slow. These findings thus indicated that if environmental behaviour changes during the cooling process of coal, coal is likely to recuperate. After 600 h, the flame dissipated, the coal temperature returned to the ambient temperature, and the test was concluded.

The development of temperature fields in coal combustion is affected by external factors, such as airflow and climate, and internal factors, such as coal quality and cracks. These result in complex nonlinear and uncontrolled temperature field variation trends. In the present study, the temperature diffusion was slow because of the poor thermal conductivity and high metamorphic degree of the selected coal. If the influence of external factors was ignored, the oxygen channel could be determined according to the coal crack to identify the distribution of the high-temperature zone and thus indicate alternations in temperature over time.

## 3.4 Semi-enclosed experimental system reliability verification

The reliability of the self-developed semi-enclosed experimental system was verified through a comparative analysis. Accordingly, TG data obtained at a heating rate of 10 °C/min were compared with experimental data derived by the system. For a clearer analysis of the oxidation thermal reaction process of coal, four characteristic temperature points were reselected according to the TG curves: high adsorption temperature ($T_a$, 110 °C), initial temperature of oxygen absorption and mass gain ($T_l$, 200 °C), maximum mass temperature ($T_m$, 306 °C), and burnout temperature ($T_f$, 589 °C). The TG experiment was divided into four stages: gas-adsorption mass-gain (initial temperature to $T_a$), degassing and dehydration mass-loss ($T_a$ to $T_l$), oxygen-absorption mass-gain ($T_l$ to $T_m$), and pyrolysis or combustion mass-loss ($T_m$ to $T_f$) stages. The changes in mass loss and the mass loss rate in each stage during the TG experiment are illustrated in Fig. 8. For the simulation of combustion development in the semi-enclosed system, the experiment was divided into five stages: initial to critical temperature, critical to dry cracking temperature, dry cracking to active temperature, active to increasing temperature, and increasing to ignition

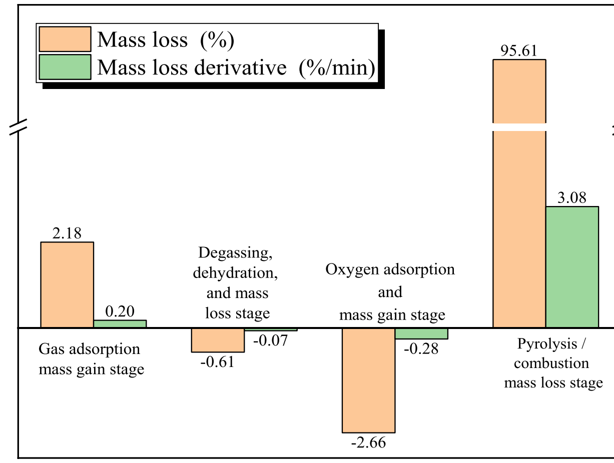


**Fig. 8** Changes in mass loss and mass loss rate in the TG experiment for Mengcun coal samples

temperature. Because the measuring points in the first layer were considerably affected by the environment, the three measuring points and high-temperature measuring points in the second layer were selected as the observation objects to determine the time required for the measuring points to react in the first to the fifth stages of the experiment. The results are depicted in Fig. 9.

Because of the similarities between the TG experiment and the simulated experiment in the semi-enclosed system, the proportional method was selected to analyse the data obtained from both experiments in order to validate the accuracy of the semi-enclosed experimental system. In the four stages of the TG experiment, the rate of mass loss was 0.02%, 0%, 0.01%, and 99.00%, and the variation trend indicated an initial increase in mass, then a decrease, and then a maximum decrease. The mass loss rate changed from fast to slow and became negative in the oxygen-absorption mass-gain stage, signifying that the mass commenced to increase, after which the increase rate dropped, and then the loss rate started to increase again in the pyrolysis or combustion mass-loss stage. Analysing the two indicated that water evaporation and desorption, oxygen absorption and mass gain, and thermal decomposition occurred. The reaction times observed at points 4, 5, and 6 in the second layer were essentially similar in the five stages of the simulation experiment conducted in the semi-enclosed system (Fig. 9a); as illustrated in Fig. 9b, the reaction times required at the high-temperature points in each layer in the first and second stages increased with the layer depth, and the differences between the reaction times observed in the other three stages were small. Comparisons of measuring points in the horizontal and vertical directions revealed that the time required in the first stage accounted for the largest proportion of the total reaction time required in all stages in the experiment conducted

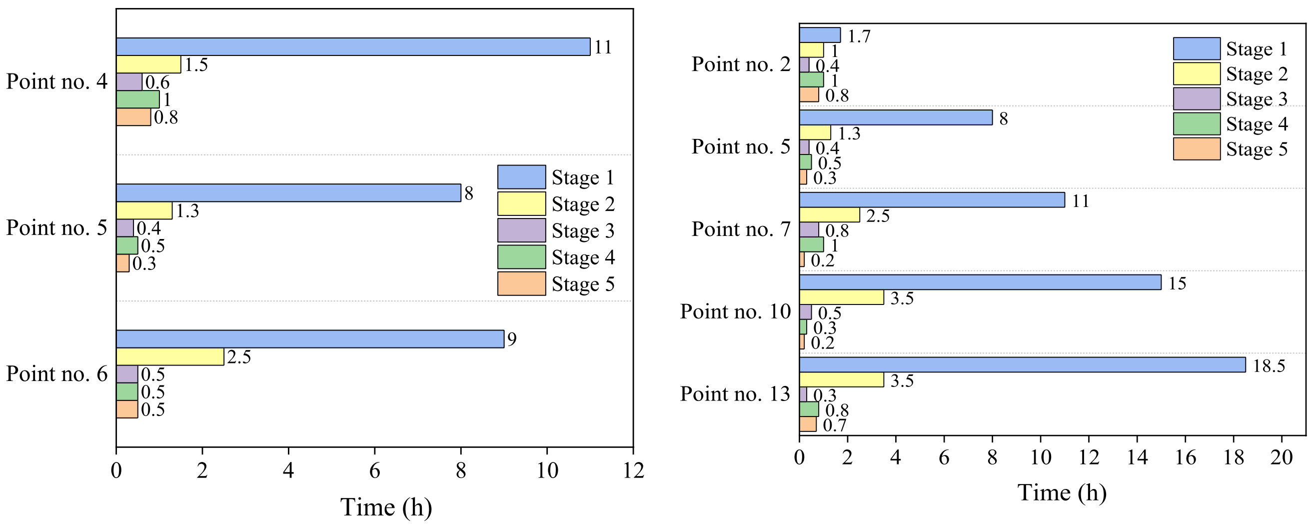


(a) Measuring points in second layer

(b) High-temperature measuring points

**Fig. 9** Time of reactions in stages 1 to 5 for Mengcun coal samples

with the semi-enclosed system. In the first and second stages, water evaporation and desorption and partial oxygen absorption and mass gain occurred; these stages were equivalent to the gas-adsorption mass-gain stage of the TG experiment, as determined from the comparison of the mass loss and mass loss rate in the TG experiment. In this stage, the mass loss and reaction time increased and the mass loss rate decreased. In the later stage, the mass loss initially decreased and then increased, but the mass loss rate continued to increase, and the time initially decreased and then increased. However, because of the simultaneous increase in reaction time in the two stages, the reaction time did not reach the initial reaction time. Therefore, the reaction times required in the various stages of the experiment in the semi-enclosed system were consistent with those required in the various stages of the TG experiment. The comparative analysis results indicated that the data obtained using the semi-enclosed system were consistent with the development and distribution coal spontaneous combustion; therefore, the system was sufficient for simulating the natural ignition of a coalfield fire.

### 3.5 Relationship between coal temperature variation and distance from measuring point

Measuring points in the same horizontal direction were selected for temperature variation evaluation. The evaluation results revealed that, over time, the temperature at the measuring points varied with the distance from the coal surface. The temperature variation results are summarised in Tables 4, 5, 6 and 7.

**Table 4** Temperature (°C) at measuring point within 50 mm from right side of furnace

| Measuring point number | Distance (mm) | Time (h) | | | |
|---|---|---|---|---|---|
| | | 6 | 12 | 18 | 24 |
| 2 | 105.0 | 389.3 | 512.3 | 621.6 | 620.3 |
| 4 | 175.0 | 17.1 | 103.4 | 444.2 | 550.8 |
| 8 | 245.0 | 10.0 | 76.5 | 211.8 | 454.2 |
| 10 | 315.0 | 8.3 | 36.9 | 101.5 | 394.4 |
| 14 | 385.0 | 6.5 | 9.7 | 53.5 | 178.0 |

**Table 5** Temperature at measuring point within 150 mm from right side of furnace

| Measuring point number | Distance (mm) | Time (h) | | | |
|---|---|---|---|---|---|
| | | 6 | 12 | 18 | 24 |
| 3 | 105.0 | 240.2 | 505.3 | 598.2 | 584.2 |
| 6 | 175.0 | 21.3 | 132.9 | 554.7 | 567.2 |
| 9 | 245.0 | 11.1 | 85.2 | 356.7 | 500.5 |
| 12 | 315.0 | 7.1 | 25.1 | 93.6 | 371.3 |
| 15 | 385.0 | 6.5 | 8.6 | 39.6 | 149.8 |

The relationship between the temperature variation and distance from the measuring points is shown in Fig. 10. The temperature variation curve was subjected to a regression analysis, and the relationship between the temperature $t$ and the distance $l$ was obtained as follows:

**Table 6** Temperature at measuring point within 50 mm from left side of furnace

| Measuring point number | Distance (mm) | Time (h) | | | |
|---|---|---|---|---|---|
| | | 6 | 12 | 18 | 24 |
| 1 | 105.0 | 96.3 | 470.8 | 532.2 | 560.1 |
| 5 | 175.0 | 21.8 | 315.3 | 583.4 | 591.5 |
| 7 | 245.0 | 16.2 | 88.6 | 389.7 | 520.0 |
| 11 | 315.0 | 7.0 | 14.8 | 85.7 | 294.7 |
| 13 | 385.0 | 7.0 | 15.2 | 58.7 | 253.0 |

**Table 7** Temperature at points in high-temperature zone

| Measuring point number | Distance (mm) | Time (h) | | | |
|---|---|---|---|---|---|
| | | 6 | 12 | 18 | 24 |
| 2 | 105.0 | 389.3 | 512.3 | 621.6 | 620.3 |
| 5 | 175.0 | 21.8 | 315.3 | 583.4 | 591.5 |
| 7 | 245.0 | 16.2 | 88.6 | 389.7 | 520.0 |
| 10 | 315.0 | 8.3 | 36.9 | 101.5 | 394.4 |
| 13 | 385.0 | 7.0 | 15.2 | 58.7 | 253.0 |

$$t = al^3 + bl^2 + cl + d, \quad (2)$$

where, $t$ represents the temperature (°C); $l$ is for the distance from the coal surface (mm); $a$, $b$, and $c$ are the regression equation coefficients; and $d$ is the regression equation intercept.

The temperature fitting curve was consistent with the regression equation at multiple measuring points. The values of $a$, $b$, $c$, and $d$ derived for the coal samples are shown in Table 8. The correlation coefficient $R^2$ value was approximately 0.98, indicating reasonable homogeneity through this regression equation.

### 3.6 Discussion

The self-developed semi-enclosed experimental system can simulate coal spontaneous combustion. On the basis of the results obtained from a comprehensive examination of the experimental process, the following observations were made. The temperature continued to decrease with time, and the temperature decreased as the coal depth increased. This occurred because the thermal conductivity of the coal was weak. With the low ambient temperature and without an external heat source, the temperature decreased gradually because of self-heating. For the Mengcun coal samples, heat accumulation required a long time in the early stage of the combustion process, and the heat transfer rate was slow, leading to a long-term fire. The temperatures observed in the first two layers of the coal samples were relatively low after 200 h, and the combustion of the surface coal was quenched. After 300 h, the temperatures observed in the third, fourth, and fifth layers were relatively low, and the combustion was completed. Because of the low temperature of the coal samples in the bottom layer of the furnace, some of these samples exhibited incomplete combustion. The combustion period of the Mengcun coal samples was 600 h, and this can be attributed to the large heat release and high moisture in the samples. Because of their high rank, the coal samples required a relatively large amount of heat in the early stage to maintain combustion, and heat generation and accumulation required a relatively long period. These processes explained the increased combustion period of the coal samples.

The analysis of the mechanism underlying the distribution of the high-temperature zone in the coal samples revealed that the high-temperature zone exhibited a downward trend. Because of the influence of pore structures, oxygen concentration, and other conditions, the high-temperature zone manifested a nonlinear movement direction. Temperature changes in the first and second layers of the coal were principally affected by environmental airflow, pores, and heat transfer. The temperatures of the samples in the first two layers were similar. The temperatures in the third, fourth, and fifth layers were affected by the pores and heat transfer, and the temperatures decreased sequentially.

According to the experimental results, the temperatures observed at the measuring points in the high-temperature zone decreased gradually with depth, which is consistent with the pattern observed in actual coalfield fires. The combustion process of actual coal fires is formed over hundreds of years, and the spread rate of most coal fires is slower than that observed a few years ago. This may be attributed to decreases in temperature at key points in high-temperature zones. Accordingly, the self-developed experimental system can capture the comprehensive spread of coalfield fires.

Regarding the temperature field distribution of loose coal, this study revealed that as the temperature at the key measuring points in the high-temperature zone decreased, the depth of the coal fire area increased. Because the semi-enclosed combustion environment in the high-temperature zone made it difficult for heat to diffuse outward and because the diffusion efficiency was low, heat generation, transfer, and diffusion were promoted, to a certain extent, during the coal combustion process. This thus explains why the outward heat diffusion rate in the semi-enclosed environment was always less than the heat generation rate in the internal combustion process. The coal–oxygen reaction formed during the combustion cycle promoted thermal oxygen coupling, which in turn promoted the reaction process; the coal fire could not always be extinguished. The analysis results also indicated that during the spread of the coal fire in the deep layer, a weak fracture environment was formed; thus, the amount and concentration of

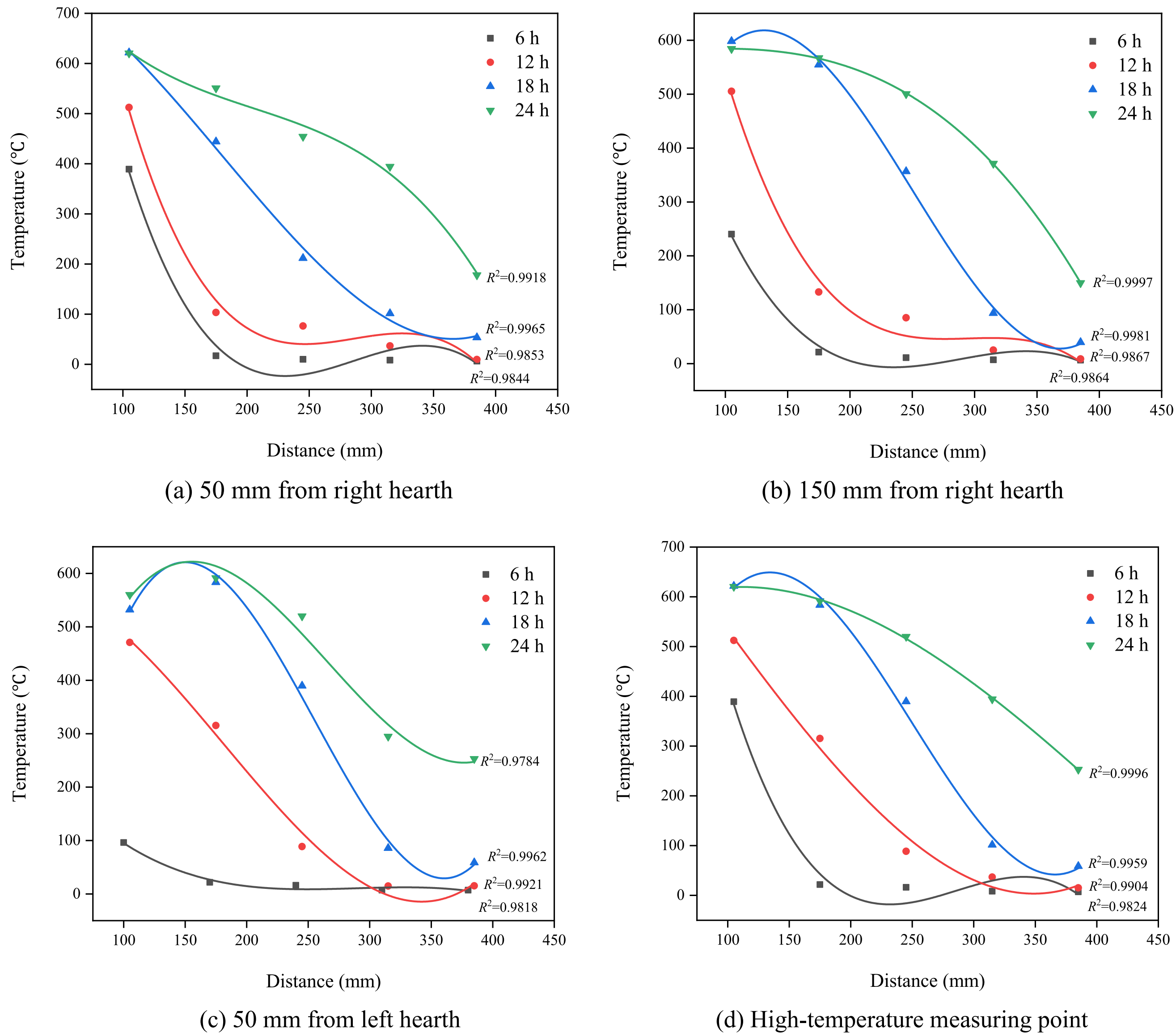


**Fig. 10** Temperature change with distance for Mengcun coal samples

infiltrated oxygen decreased, and the advancement of the coal–oxygen reaction was slow, resulting in a decreased temperature in the high-temperature zone. Furthermore, the weak fracture environment promoted the active transport of heat, resulting in the continuous spread of the high-temperature zone to greater depths. The weak fracture environment prevented the massive diffusion of oxygen, and the reaction of coal with oxygen was not the main factor for the deep spread of the high-temperature zone. Accordingly, the current findings imply that mitigation efforts should focus on the extraction of heat from combustion areas; the findings could also provide a theoretical basis for coal fire prevention and control.

## 4 Conclusions

On the basis of the study findings, the following conclusions were drawn:

(1) The self-developed semi-enclosed experimental system can simulate the propagation and evolution of high-temperature zones in coal combustion.
(2) Because the combustion cycle of the coal samples used in this study was 600 h, the first high-temperature zone in the combustion process appeared at 5 h and moved to the bottom of the experimental furnace at 26 h. The high-temperature zone exhibited a nonlinear trend

**Table 8** Values of *a*, *b*, *c*, and *d* in regression equations derived for Mengcun coal samples

| Point | Time (h) | $a$ ($\times 10^{-5}$) | $b$ | $c$ | $d$ |
|---|---|---|---|---|---|
| Points in 50 mm from the right side | 6 | −8.873 | 0.076 | −20.936 | 1846.278 |
| | 12 | −8.980 | 0.077 | −21.567 | 2026.505 |
| | 18 | 2.850 | −0.015 | −0.176 | 780.228 |
| | 24 | −3.146 | 0.019 | −4.793 | 950.001 |
| Points in 150 mm from the right side | 6 | −4.988 | 0.043 | −12.002 | 1079.023 |
| | 12 | −6.829 | 0.060 | −17.729 | 1774.490 |
| | 18 | 8.834 | −0.066 | 12.796 | −120.615 |
| | 24 | −1.035 | $7.340 \times 10^{-4}$ | 0.156 | 572.001 |
| Points in 50 mm from the left side | 6 | −1.450 | 0.013 | −3.558 | 339.796 |
| | 12 | 3.533 | −0.019 | 0.722 | 569.948 |
| | 18 | 1.268 | −0.097 | 20.562 | −706.832 |
| | 24 | 6.961 | −0.056 | 12.216 | −196.461 |
| High-temperature points | 6 | −8.632 | 0.074 | −20.433 | 1812.511 |
| | 12 | 1.450 | −0.003 | −3.202 | 869.784 |
| | 18 | 9.740 | −0.073 | 14.361 | −197.071 |
| | 24 | 6.535 | −0.009 | 1.732 | 528.012 |

under the influence of the internal properties of coal and external environmental factors.

(3) The temperature at the key point in the high-temperature zone peaked relative to the ignition temperature. The temperature growth rate at this point decreased linearly as the depth increased; the time associated with the swift decline in oxygen concentration at key points in the high-temperature zone increased gradually with depth.

(4) The current findings imply that measures for preventing and controlling coalfield fires with a wide depth and range should focus on heat extraction from the combustion area. The findings could provide a theoretical basis for preventing and controlling coalfield fires. On this basis, research on underground coal fire source identification and inversion technology can be carried out.

**Acknowledgements** Financial support for this study was kindly provided by the National Natural Science Foundation Project of China (No. 51804246, No. 52174202), Natural Science Foundation of Xinjiang Province (No. 2019D01C057), and the Youth Talent Promotion Program of Shaanxi University Association for Science and Technology (No. 20200425).

**Author contributions** JZ: Supervision, Validation, Investigation, Funding acquisition, Project administration. HM: Conceptualisation, Data curation, Writing–original draft. TG: Formal analysis. YZ: Methodology. JD: Funding acquisition. JS: Resources, Writing–review & editing. QZ: Project administration. C-MS: Writing–review & editing.

## Declarations

**Competing interests** The authors declare that they have no known competing financial interests or personal relationships that could have appeared to influence the work reported in this paper.



## References

Alipour M, Alizadeh B, Jahangard A, GandomiSani A (2021) Wildfire events at the Triassic-Jurassic boundary of the Tabas Basin, Central Iran. Int J Coal Sci Technol 8(5):897–907. https://doi.org/10.1007/s40789-021-00436-2

Elick JM (2013) The effect of abundant precipitation on coal fire subsidence and its implications in Centralia. PA Int J Coal Geol 105(1):110–119

Fan L, Liu S (2021) Respirable nano-particulate generations and their pathogenesis in mining workplaces: a review. Int J Coal Sci Technol 8(2):179–198. https://doi.org/10.1007/s40789-021-00412-w

Gehin E, Skelton B, Vallero DA (2016) Air pollution control and waste management. Process Saf Environ Prot 101:1

Guo J, Wen H, Zheng XZ, Liu Y, Cheng XJ (2019) A method for evaluating the spontaneous combustion of coal by monitoring various gases. Process Saf Environ Prot 126(1):223–231

Hao Y, Liu Y, Weng JH, Gao Y (2016) Does the environmental kuznets curve for coal consumption in China exist new evidence from spatial econometric analysis. Energy 114(1):1214–1223

Huang JJ, Bruining J, Wolf K (2001) Modeling of gas flow and temperature fields in underground coal fires. Fire Safety J 36(5):477–489

Ide ST, Orrjr F (2011) Comparison of methods to estimate the rate of $CO_2$ emissions and coal consumption from a coal fire near Durango, CO. Int J Coal Geol 86(1):95–107

Kuenzer C, Zhang JZ, Sun YL, Jia Y, Dech S (2012) Coal fires revisited: The Wuda coal field in the aftermath of extensive coal fire research and accelerating extinguishing activities. Int J Coal Geol 102:75–86

Ma L, Guo RZ, Gao Y, Ren LF, Wei GM, Li CH (2019) Study on coal spontaneous combustion characteristics under methane-containing atmosphere. Combust Sci Technol 191:1456–1472

Ma L, Guo RZ, Wu MM, Wang WF, Wei GM (2020) Determination on the hazard zone of spontaneous coal combustion in the adjacent gob of different mining stages. Process Saf Environ Prot 142(4):370–379

Nyakundi MM (2014) Energy and the Environment: the relationship between coal production and the environment in China. Nat Resour Res 23(2):285–298

Onifade M, Genc B, Bada S (2020) Spontaneous combustion liability between coal seams: a thermogravimetric study. Int J Min Sci Techno 30(5):691–698

Pandey B, Agrawal M, Singh S (2014) Assessment of air pollution around coal mining area: emphasising on spatial distributions, seasonal variations and heavy metals, using cluster and principal component analysis. Atmos Pollut Res 5:79–86

Qin BT, Wang HT, Yang JZ, Liu LZ (2016) Large-area goaf fires: a numerical method for locating high-temperature zones and assessing the effect of liquid nitrogen fire control. Environ Earth Sci 75(21):1396

Rosema A, Guan H, Veld H (2001) Simulation of spontaneous combustion, to study the causes of coal fires in the Rujigou Basin. Fuel 80(1):7–16

Roy D, Gautam S, Singh P, Singh G, Kanti B, Aditya D, Patra K (2016) Carbonaceous species and physicochemical characteristics of $PM_{10}$ in coal mine fire area—a case study. Air Qual Atmos Hlth 9:429–437

Saini V, Gupta RP, Arora MK (2016) Environmental impact studies in coalfields in India: a case study from Jharia coal-field. Renew Sust Energy Revr 53:1222–1239

Song ZY, Zhu HQ, Tan B, Wang HY, Qin XF (2014) Numerical study on effects of air leakages from abandoned galleries on hill-side coal fires. Fire Safety J 69:99–110

Song YW, Yang SQ, Xu Q, Cai JW, Hu XC, Sang NW, Zhang ZC (2019) Effect of low-temperature oxidation of coal with different metamorphic degrees on coal quality characteristics and outburst comprehensive index. Process Saf Environ Prot 132:142–152

Song ZY, Huang XY, Jiang JC, Pan XH (2020) A laboratory approach to $CO_2$ and CO emission factors from underground coal fires. Int J Coal Geol 219:103382

Song JJ, Deng J, Zhao JY, Zhang YN, Wang CP, Shu CM (2021) Critical particle size analysis of gas emission under high-temperature oxidation of weathered coal. Energy 214:118995

Stracher GB, Taylor TP (2004) Coal fires burning out of control around the world: thermodynamic recipe for environmental catastrophe. Int J Coal Geol 59(1):7–17

Sun XF, Shao HY, Xiang XY, Yuan LG, Zhou YZ, Xian W (2020) A coupling method for eco-geological environmental safety assessment in mining areas using PCA and catastrophe theory. Nat Resour Res 29(3):4133–4148

Tan B, Zhang FC, Zhang QS, Wei HY, Shao ZZ (2019) Fire fighting of subsurface coal fires with comprehensive techniques for detection and control: a case study of the Fukang coalfire in the Xinjiang region of China. Environ Sci Pollut R 26:29570–29584

Taraba B, Michalec Z (2011) Effect of longwall face advance rate on spontaneous heating process in the gob area–CFD modelling. Fuel 90(8):2790–2797

Wang CP, Xiao Y, Li QW, Deng J, Wang K (2018) Free radicals, apparent activation energy, and functional groups during low-temperature oxidation of Jurassic coal in Northern Shaanxi. Int J Min Sci Techno 28(3):469–475

Wang K, Fan HB, Gao P, He YZ, Yang C (2020a) Influence of water content on the coal spontaneous combustion behavior during low-temperature pre-pyrolysis processes. Combust Sci Technol 193(12):1–12

Wang ZY, Cheng YP, Wang L, Zhou HX (2020b) Characterisation of pore structure and the gas diffusion properties of tectonic and intact coal: implications for lost gas calculation. Process Saf Environ Prot 135(1):12–21

Wessling S, Kuenzer C, Kessels W, Wuttke MW (2008) Numerical modeling for analysing thermal surface anomalies induced by underground coal fires. Int J Coal Geol 74(3–4):175–184

Wolf K, Bruining H (2007) Modeling the interaction between underground coal fires and theirs roof rocks. Fuel 86(17–18):2761–2777

Xia TQ, Zhou FB, Liu JS, Kang JH, Gao F (2014) A fully coupled hydro-thermo-mechanical model for the spontaneous combustion of underground coal seams. Fuel 125(125):106–115

Xiao Y, Lu JH, Wang CP, Deng J (2016) Experimental study of high-temperature fracture propagation in anthracite and destruction of mudstone from coalfield using high-resolution microfocus x-ray computed tomography. Rock Mech Rock Eng 49(9):3723–3734

Xu J, Zhou M, Li HL (2018a) The drag effect of coal consumption on economic growth in China during 1953–2013. Resour Consery Recy 129:326–332

Xu Q, Yang SQ, Tang ZQ, Cai JW, Zhong Y, Zhou BZ (2018b) Free radical and functional group reaction and index gas CO emission during coal spontaneous combustion. Combust Sci Technol 190(5):834–848

Xu Q, Yang SQ, Yang WM, Tang ZQ, Zhou BZ (2020) Micro-structure of crushed coal with different metamorphic degrees and its low-temperature oxidation. Process Saf Environ Prot 140:330–338

Yuan L, Smith AC (2007) Computational fluid dynamics modeling of spontaneous heating in longwall gob areas. Trans Soc Min Metall Explor 322:37–44

Zhang J, An JY, Wen ZH, Zhang KX, Mamun NAA (2020) Numerical investigation of coal self-heating in longwall goaf considering airflow leakage from mining induced crack. Process Saf Environ Prot 134:353–370

Zhao JY, Deng J, Chen L, Wang T, Song JJ, Zhang YN, Shu CM, Zeng Q (2019a) Correlation analysis of the functions groups and exothermic characteristic of bituminous coal molecules during high-temperature oxidation. Energy 181:136–147

Zhao JY, Deng J, Wang T, Song JJ, Zhang YN, Shu CM, Zeng Q (2019b) Assessing the effectiveness of a high-temperature-programmed experimental system for simulating the spontaneous combustion properties of bituminous coal through thermokinetic analysis of four oxidation stages. Energy 169(15):587–596

Zhao JY, Wang T, Deng J, Shu CM, Zhang YX (2020) Microcharacteristic analysis of $CH_4$ emissions under different conditions during coal spontaneous combustion with high-temperature oxidation and in situ FTIR. Energy 209(9):118494